Glass Struct. Eng. (2022) 7:121–137
https://doi.org/10.1007/s40940-022-00184-y

RESEARCH PAPER

Evaluation methods for surface compression stress measurements with unknown principle stress directions

Kerstin Thiele · Steffen Müller-Braun · Jens Schneider

Received: 1 March 2022 / Accepted: 13 June 2022 / Published online: 1 August 2022

Abstract The birefringent properties of glass can be well utilized for non-destructive testing of thermally tempered glass. The surface compression stress as well as the compression zone depth of thermally tempered glass is commonly measured with a scattered light polariscope. The measurement with scattered light polariscope provides information about stresses acting perpendicular to the measurement direction. Therefore, the measurement depends on the direction. In order to make a statement about the rough level of the prestress, a measurement in one direction can be sufficient, assuming an isotropic stress state and a relatively homogeneous distribution of the surface compression stress. However, in order to be able to make a more detailed statement about a non-isotropic stress state, measurements in up to four directions are necessary. Information about the direction of principal stresses and differences of principal stresses can then be evaluated. In the present work, it is investigated which deviations can be expected by measurements performed in only one direction or by measurements using up to four directions. For this purpose, five methods are introduced, which deviate in the assumptions made for the current stress state. The methods are compared using measurements on thermally tempered glass in a four-point bending test and on thermally tempered glass specimens without any external load.

K. Thiele (✉) · S. Müller-Braun · J. Schneider
Institute of Structural Mechanics and Design (ISM+D), Technical University of Darmstadt, Darmstadt, Germany

Keywords Thermally tempered glass · Scattered light polariscope · Principal stresses

1 Introduction

As glass is a birefringent material, when applied to stress, photoelastic methods are a good tool to identify the current stress state in glass products. In the container glass industry, this is used to investigate residual stresses in the container, as these residual stresses can lead to unexpected failure of the container during use (Erraprat 2010). In the flat glass industry, photoelastic methods are used to determine residual stresses in float glass or thermally tempered glass.

In the case of thermally tempered flat glass in general, the surface compression stress, the compression zone depth, the edge membrane stress as well as the homogeneity of residual stresses are of interest. When the residual stresses resulting from the thermal tempering process show a low homogeneity, due to the stress-induced birefringence of glass, interference colors can become visible for the observer when installed on site. This physical effect is also called optical anisotropy effects in the building industry. To evaluate the optical quality with respect to anisotropy effects, anisotropy scanners can be used, which are either polarimeters or polariscopes. Current research results on optical anisotropy effects are described in (Dix 2021a). In DIN SPEC 18,198:2022-05 (2022) measurement techniques

are described and evaluation zones, evaluation methods and quality classes are defined. A higher quality class reduces the risk of visible anisotropy effects. A summary of photoelastic methods allowing full-field measurements of architectural glass is given in (Dix 2022).

To evaluate the surface compression stress and the corresponding surface compression zone depth at discrete points, a scattered light polariscope (SCALP) can be used. This is of interest, for example, for the prediction of the fracture pattern, see (Nielsen et al. 2010, Pour-Moghaddam 2019). Lohr (2020) has used measurements performed with SCALP-04 and StrainScope to determine the residual stresses of thermally tempered glass before and after regrinding the edges. Dix et al. (2021b) have analysed the residual stresses at holes near edges in thermally tempered glass using a SCALP-05 and two other full-field methods. Chen et al. (2013) and Karvinen et al. (2019) have used SCALP measurements to perform full-field measurements on relatively small areas to investigate the homogeneity and the isotropy of the residual stress state after thermal tempering. For full-field measurements with SCALP, a high number of discrete points in short distance need to be evaluated.

Nielsen et al. (2021) have compared more than 600 SCALP measurements and found a dependency of compression zone depth on glass thickness. The specimens showed a larger compression zone depth with increasing nominal thickness. Thiele et al. (2022) has found a dependency of surface compression zone depth regarding the two sides of glass panes. The specimens showed a slightly larger compression zone depth on the side, which had contact with the rollers during thermal tempering process. A higher standard deviation for heat strengthened glass was found.

Zaccaria and Overend (2020) investigated accuracy and precision of SCALP measurements for different photoelastic constants. Their experimental results fitted best for a photoelastic constant $C = 3.01$ TPa^{-1} and showed an accuracy of ± 4.7 MPa and a precision of ± 3.9 MPa. Unfortenately, no information about the device used and the fitting method used are given.

In this contribution, the method for evaluating surface compression stress by means of SCALP is considered in more detail. The calculation of the stresses from the measurement data depends on the orientation of the measurement to the principal stress directions. These interrelationships will be examined. After that, five evaluation methods are presented. The first method assumes isotropic stress state, the second method assumes known principal stress directions. The other three methods do not assume isotropic stress state or known principal stress states. All methods are compared on the basis of measurements on thermally tempered flat glass without external load and within four-point bending test. It was found, that principal stresses evaluated by the five methods show different results with standard deviations of up to 2.5 MPa. The more assumptions are made to reduce complexity of the problem, the more deviates the solution from expected results.

2 Basics regarding scattered light polariscope

Figure 1a shows the setup of the SCALP schematically. A polarized laser is guided through a prism at a defined angle α into the glass sample. The angle α corresponds to the angle between the laser and the vertical axis and is usually used in the manufacturer's descriptions. The angle β corresponds to the angle between laser and the horizontal axis and is used for calculations in this work. In Fig. 1a, the axes x, y, z, which create a global coordinate system that can be aligned with the edges of the specimen, and the axes η, ζ, y creating a local coordinate system are introduced. In Fig. 1b, the axes x, y, z are shown from a top view. Additional axes p and q are introduced, which correspond to additional directions for measurements if measurements in up to four directions are chosen to evaluate the current stress state. Figure 1c shows the coordinate systems corresponding to measurements in x- and y-directions.

The measurement shown in Fig. 1a is a measurement in the direction of the x-axis. The intensity of the scattering of the polarized laser along the laser path on the η-axis is then recorded laterally. From the intensity of the scattering the retardation $\delta(\eta)$ can be calculated, for which in turn applies

$$\delta(\eta) = C \int_{\eta_0}^{\eta} (\sigma_{s,1} - \sigma_{s,2}) d\eta. \tag{1}$$

Thus, the retardation depends on the photoelastic constant C, as well as on the secondary principal stresses $\sigma_{s,1}$ and $\sigma_{s,2}$ in the ζy-plane perpendicular to the laser.

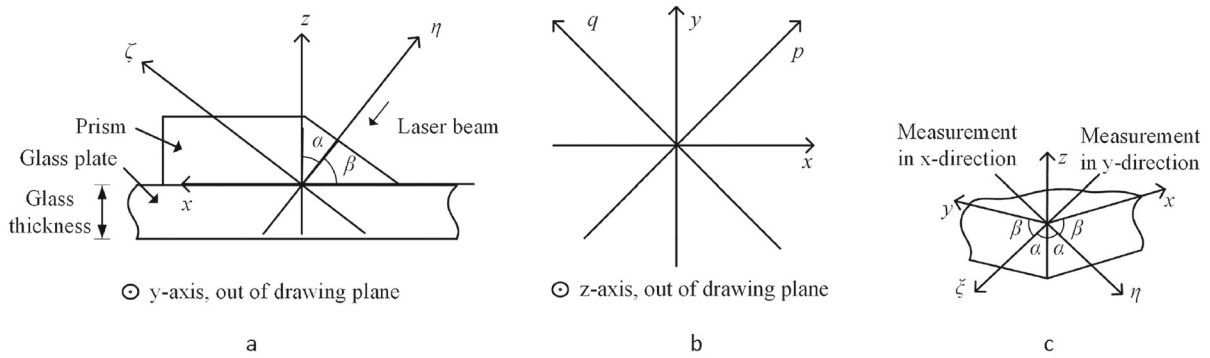

Fig. 1 **a** Schematic draw of SCALP measuring device and **b** coordinate system x–y and **c** schematic draw of measurement in x- and y-direction. (according to GlassStress) ©Thiele

In this work, the secondary principal stresses, i.e. principal stresses in a defined plane, are given the additional subscript s to clearly communicate when secondary and when principal stresses of the three-dimensional stress state are meant. Since the stresses in the glass thickness direction can be neglected in thermally tempered glass, the three-dimensional stress state is converted into a two-dimensional stress state. This results in the principal stresses σ_1 and σ_2 instead of σ_2 and σ_3 for the compression stresses at the surfaces of thermally tempered glass.

To determine the principal stresses of the three dimensional stress state, it is useful to first define the stress state in a global coordinate system:

$$\boldsymbol{\sigma}_{xyz} = \begin{pmatrix} \sigma_x & \tau_{xy} & \tau_{xz} \\ \tau_{xy} & \sigma_y & \tau_{yz} \\ \tau_{xz} & \tau_{yz} & \sigma_z \end{pmatrix}. \tag{2}$$

By rotating around the y-axis by the angle β counterclockwise, the stress state in Eq. 2 can be transformed into the local coordinate system:

$$\boldsymbol{\sigma}_{\eta y\zeta} = \begin{pmatrix} \sigma_x \cos^2(\beta) + 2\tau_{xz}\cos(\beta)\sin(\beta) + \sigma_z \sin^2(\beta) & c & a \\ c & \sigma_y & b \\ a & b & \sigma_z \cos^2(\beta) + \sigma_x \sin^2(\beta) - 2\tau_{xz}\sin(\beta)\cos(\beta) \end{pmatrix},$$

with $a = -\sigma_x \sin(\beta)\cos(\beta) - \tau_{xz}\sin^2(\beta) + \tau_{xz}\cos^2(\beta) + \sigma_z \sin(\beta)\cos(\beta)$,
$b = -\tau_{xy}\sin(\beta) + \tau_{yz}\cos(\beta) - \tau_{xy}\sin(\beta) + \tau_{yz}\cos(\beta)$,
$c = \tau_{xy}\cos(\beta) + \tau_{yz}\sin(\beta)$ (3)

By solving the eigenvalue problem of the matrix from Eq. 3, the secondary principal stresses $\sigma_{s,1}$ and $\sigma_{s,2}$ can be determined as a function of the stresses in the global coordinate system. Since solving the eigenvalue problem for the general stress state is complex, assumptions of the stress state are chosen to simplify the calculation. For example, $\sigma_z = \tau_{xz} = \tau_{yz} = 0$ is a common assumption for the stress state of thermally tempered glass far away from the edges.

The retardations calculated from the measured data are approximated by fitting a function. The derivative of this function is directly proportional to the sought secondary principal stresses:

$$d\delta(\eta)/d\eta = C\left(\sigma_{s,1} - \sigma_{s,2}\right). \tag{4}$$

To determine the principal stresses or the stresses in the x- and y-directions, several measurements may be necessary depending on the assumption of the stress state, see Sect. 3. Further information on the functionality of the SCALP can be obtained from (Aben 1993, Anton 2003, Aben 2008, Anton 2015).

3 Evaluation methods of principal stresses

Depending on the expected stress state in the glass specimen, simplifications can be made to determine the secondary principal stresses, as addressed in the previous

section. In this section, different evaluation methods and their assumptions are described.

3.1 Isotropic stress state

To reduce complexity, the stress state in the centre of a thermally toughened glass sheet may be assumed to be isotropic. In this case, in addition to the usual assumptions for thermally tempered glass ($\sigma_z = \tau_{xz} = \tau_{yz} = 0$), also the following assumptions apply: $\sigma_x = \sigma_y$ and $\tau_{xy} = 0$. The stresses in the local coordinate system for a measurement in x-direction are then given by

$$\boldsymbol{\sigma}_{\eta y\zeta} = \begin{pmatrix} \sigma_x \cos^2(\beta) & 0 & -\sigma_x \sin(\beta)\cos(\beta) \\ 0 & \sigma_x & 0 \\ -\sigma_x \sin(\beta)\cos(\beta) & 0 & \sigma_x \sin^2(\beta) \end{pmatrix}. \quad (5)$$

This results in the following secondary principal stresses in $y\zeta$-plane:

$$\boldsymbol{\sigma}_{y\zeta} = \begin{pmatrix} \sigma_x & 0 \\ 0 & \sigma_x \sin^2(\beta) \end{pmatrix}. \quad (6)$$

With Eq. 4, this gives the following relationship between stresses and retardations from which the stress state can be fully determined (Anton 2015):

$$\sigma_y(\eta) = \sigma_x(\eta) = \frac{\delta'(\eta)}{C\cos^2(\beta)}. \quad (7)$$

In case of isotropic stress state, σ_x and σ_y correspond to the principal stresses. Only one measured direction is necessary to determine the current stress state in this case.

3.2 Known principal stress directions

For example, in a four-point bending test, the principal stress directions are known. For thermally tempered glass without external load, no statement can be made about the principal stress direction, since a complex distribution of heat is present in the toughening process, which can also cause varying principal stress directions. To reduce the complexity, however, it can be assumed that the principal stress directions are known.

If the principal stress directions are known ($\tau_{xy} = 0$), and $\sigma_z = \tau_{xz} = \tau_{yz} = 0$ can be assumed, Eq. 3 for the measurement in x-direction simplifies as follows:

$$\boldsymbol{\sigma}_{\eta y\zeta} = \begin{pmatrix} \sigma_x \cos^2(\beta) & 0 & -\sigma_x \sin(\beta)\cos(\beta) \\ 0 & \sigma_y & 0 \\ -\sigma_x \sin(\beta)\cos(\beta) & 0 & \sigma_x \sin^2(\beta) \end{pmatrix}. \quad (8)$$

The stresses in the x- and y-directions, which correspond to the principal stress directions, can be calculated by using measurements in the two principal stress directions. With Eq. 4 for these two directions applies (Anton 2015):

$$\begin{aligned} \sigma_y(\eta) - \sigma_x(\eta)\sin^2(\beta) &= \frac{\delta'(\eta)}{C} \text{ and} \\ \sigma_x(\xi) - \sigma_y(\xi)\sin^2(\beta) &= \frac{\delta'(\xi)}{C}. \end{aligned} \quad (9)$$

From these relationships, the two stresses σ_x and σ_y can be determined.

3.3 Unknown principal stress directions and non-isotropic stress state

Anisotropy effects are a common visible effect with thermally tempered glass (Fachverband Konstruktiver Glasbau e.V. 2019). For SCALP measurements this indicates, that principal stresses in the plane perpendicular to light path do not equal each other. As the thermal conditions in the tempering process are complex, no information can be given on principal stress directions. For SCALP data preparation, in case of thermally tempered glass with anisotropies, the conditions $\sigma_z = \tau_{xz} = \tau_{yz} = 0$ can be used. For the measurement in x-direction, Eq. 3 simplifies to:

$$\boldsymbol{\sigma}_{\eta y\zeta} = \begin{pmatrix} \sigma_x \cos^2(\beta) & \tau_{xy}\cos(\beta) & -\sigma_x \sin(\beta)\cos(\beta) \\ \tau_{xy}\cos(\beta) & \sigma_y & -\tau_{xy}\sin(\beta) \\ -\sigma_x \sin(\beta)\cos(\beta) & -\tau_{xy}\sin(\beta) & \sigma_x \sin^2(\beta) \end{pmatrix} \quad (10)$$

As the stresses σ_x, σ_y, τ_{xy} are unknown parameters, a minimum of three measurements must be performed. In the following, three methods are described. Two of the methods use three measured directions, one of them uses four measured directions.

3.3.1 Method using four measured directions

Firstly, a method using four measured directions is introduced. This method is described in SCALP manual for the case of unknown principal stress directions. This method includes, additional to Eq. 9, the following relationships for the two additional measured directions p and q with coordinate axis λ and ζ, respectively,(Anton 2015):

$$\begin{aligned}\sigma_p(\zeta) - \sigma_q(\zeta)\sin^2(\beta) &= \frac{\delta'(\zeta)}{C}, \text{ and}\\ \sigma_q(\lambda) - \sigma_p(\lambda)\sin^2(\beta) &= \frac{\delta'(\lambda)}{C},\end{aligned} \tag{11}$$

As the relationships presented in Eqs. 9 and 11 are conducted using the matrix in Eq. 8 instead of the matrix in Eq. 10, the contribution of τ_{xy} to the measured retardation is neglected while evaluating σ_x, σ_p, σ_y and σ_q.

The principal stresses are calculated using the following relationships:

$$\tau_{xy} = \frac{1}{2}\left(\sigma_p - \sigma_q\right) \tag{12}$$

$$\sigma_1, \sigma_2 = \frac{\sigma_x + \sigma_y}{2} \pm \sqrt{\left(\frac{\sigma_x - \sigma_y}{2}\right)^2 + \tau_{xy}}. \tag{13}$$

3.3.2 System of nonlinear equations using 3 measured directions

Secondly, a method is introduced which was evaluated by solving the eigenvalue problem with the matrix in Eq. 10. The secondary principal stresses in ζy-plane for measurement in x-direction result to

$$\sigma_{s,1}(\eta) = \frac{\sigma_y(\eta) + \sigma_x(\eta)\cos^2(\beta) + \sqrt{\sigma_x^2(\eta)\cos^4(\beta) + 4\tau_{xy}^2(\eta)\cos^2(\beta) + \sigma_y^2(\eta) - 2\sigma_x(\eta)\sigma_y(\eta)\cos^2(\beta)}}{2}, \tag{14}$$

$$\sigma_{s,2}(\eta) = \frac{\sigma_y(\eta) + \sigma_x(\eta)\cos^2(\beta) - \sqrt{\sigma_x^2(\eta)\cos^4(\beta) + 4\tau_{xy}^2(\eta)\cos^2(\beta) + \sigma_y^2(\eta) - 2\sigma_x(\eta)\sigma_y(\eta)\cos^2(\beta)}}{2}. \tag{15}$$

For each measurement direction, the secondary principal stresses depend on $\sigma_x, \sigma_y, \tau_{xy}$. Using the relationships of the secondary principal stresses of three measurement directions (x-, y- and p-direction) given in Eqs. 14 and 15 as well as the relationship given in Eq. 4, a system of nonlinear equations is obtained:

$$\begin{aligned}\sigma_{s,1}(\eta) - \sigma_{s,2}(\eta) &= \frac{\delta'(\eta)}{C},\\ \sigma_{s,1}(\xi) - \sigma_{s,2}(\xi) &= \frac{\delta'(\xi)}{C} \text{ and}\\ \sigma_{s,1}(\zeta) - \sigma_{s,2}(\zeta) &= \frac{\delta'(\zeta)}{C},\end{aligned} \tag{16}$$

This system of equations can be solved by using, for example, the Newton method, which is described for example in (Zeidler 2013). By using this method, only three measured directions are necessary to evaluate the current stress state in the specimen without any additional assumptions but $\sigma_z = \tau_{xz} = \tau_{yz} = 0$.

3.3.3 Simplified method using three measured directions

Thirdly, a simplified method is introduced. Here, for each measured direction stresses are calculated assuming isotropic stress state accordingly to the method described in Sect. 3.1. This is done for three measured directions, see Eq. 17.

$$\begin{aligned}\sigma_y(\eta) &= \frac{\delta'(\eta)}{C\cos^2(\beta)}, \quad \sigma_x(\xi) = \frac{\delta'(\xi)}{C\cos^2(\beta)},\\ \sigma_p(\zeta) &= \frac{\delta'(\zeta)}{C\cos^2(\beta)}.\end{aligned} \tag{17}$$

Principal stresses can then be evaluated easily by using the following equations, compare (Gross 2014):

$$\tau_{xy} = \sigma_p - \frac{\sigma_y - \sigma_x}{2}, \tag{18}$$

$$\varphi_1 = \frac{1}{2}\arctan\left(\frac{2\tau_{xy}}{\sigma_x - \sigma_y}\right), \varphi_2 = \varphi_1 + \frac{\pi}{2}, \tag{19}$$

$$\sigma_1 = \frac{\sigma_x + \sigma_y}{2} + \frac{\sigma_x - \sigma_y}{2}\cos(2\varphi_1) + \tau_{xy}\sin(2\varphi_1), \tag{20}$$

$$\sigma_2 = \frac{\sigma_x + \sigma_y}{2} + \frac{\sigma_x - \sigma_y}{2}\cos(2\varphi_2) + \tau_{xy}\sin(2\varphi_2). \tag{21}$$

For this method, three measurement directions (x-, y- and p-direction) are necessary. As in Eq. 17 an isotropic stress state is assumed for each measured direction, this is not an exact solution.

4 Experiment

For analysing the different methods, thermally tempered flat glass without any external load as well as loaded within a four-point bending test were investigated.

4.1 Thermally tempered glass

The thermal tempering process is described, for example, in (Schneider 2016). The result of the tempering process is a parabolic stress state with compressive stresses at the surfaces and tensile stresses in the centre of the glass. A homogeneous heating and cooling of a glass pane is not possible, since local differences in the thermal process occur due to the rollers on which the glass is transported, the nozzles from which air flows for cooling and the complex heat distribution in the furnace. Optical anisotropy effects are a visible effect of the local differences in the thermal process. These optical effects occur when the principal stresses are anisotropic, that is, $\sigma_1 \neq \sigma_2$.

Since stresses mainly occur in the x- and y-directions, stresses in the z-direction can be neglected. A statement about the principal stress directions at each point of the glass sheet is not possible due to the complex thermal process.

Details of the five specimens investigated in this work are summarized in Table 1. Specimens 1 to 4 were investigated without any external load, specimen 5 was investigated in a four-point bending test. Specimens 1 to 4 were measured at 21 positions per specimen. Only 6 positions per specimen are discussed in this work. The numbers in braces indicate the row numbers of results given in Table 3.

4.2 Four-point bending test

Figure 2a shows the set up for the four-point bending test, which was performed inverted in order to set up the SCALP-05. A universal testing machine by ZWICK ROELL and its implemented load cell was used to apply the external forces. In this way, tensile stresses were applied to the upper surface of the specimen. Figure 2b shows static system, dimensions and the moment distribution.

Principal stress directions are known in this case. Stresses due to external load add to residual stresses from thermal tempering. As the SCALP is placed on the top side, stresses in x-direction reduce due to the external load. In this work stresses due to transverse strain are neglected.

4.3 SCALP Measurement details

Before testing, the specimens were cleaned with isopropanol. For the testing on thermally tempered glass without any external load, the specimens were placed on a paper and measurements were performed in one setup. For this setup, the four measured directions x, p, y, q were performed, where the directions x and y were aligned to the specimen edges. Three repetitions per measured direction were performed. The measured directions and the rotatable plate used for easier positioning of the SCALP are shown in Fig. 3b.

The specimen investigated in four-point bending test was marked and a strain gauge was applied before being installed, see Fig. 3a. For an easier rotation of SCALP within the four-point bending test, the rotatable plate shown in Fig. 3b was used. The SCALP was placed in the middle of the glass pane. At this location, 8 measurements in two setups, indicated in black and red coordinate systems in Fig. 3b, were performed for each load step. The first setup (black) consists of measurement directions x, p, y and q, where the directions x

Table 1 List of investigated glass specimens. FT refers to fully tempered glass (surface compression stresses above 90 MPa). HSG refers to heat strengthened glass (surface compression stresses between 30 and 60 MPa). Number of measurement locations on the specimen and number of applied load steps are given. Numbers in braces in column 6 refer to results given in Table 3. Measurement setups describe the number of different coordinate systems used

Specimen	Dimensions [mm]	Nom. thickness [mm]	Glass type	FT / HSG	No. of measured locations (ref. to Table 3)	No. of applied load steps	Setups
1	750 × 1500	8	Soda lime	FT	21 (1–6)	0	1 (0°)
2	750 × 1500	10	Soda lime	FT	21 (7–12)	0	1 (0°)
3	750 × 1500	8	Soda lime	HSG	21 (13–18)	0	1 (0°)
4	750 × 1500	12	Soda lime, low iron	HSG	21 (19–24)	0	1 (0°)
5	100 × 500	6	Soda lime	FT	1	16	2 (0° & 15°)

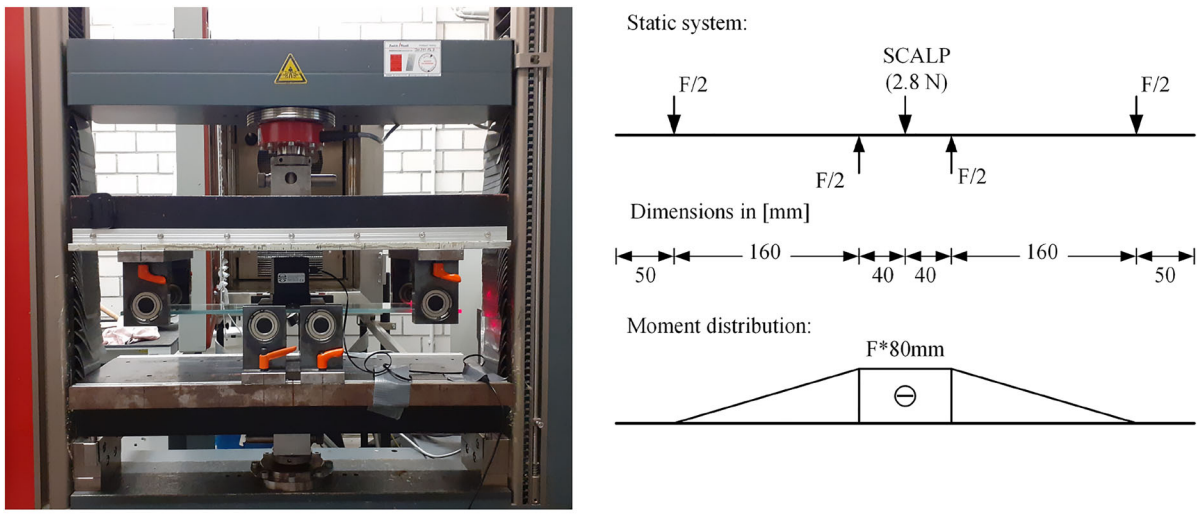

Fig. 2 Four-point bending test: **a** Test set up and **b** Static system, dimensions and moment distribution. ©Thiele

and y were aligned to the specimen edges. The second setup (red) is rotated by 15° and consists of the measured directions 15, 60, 105 and 150. Each measured direction was repeated three times. As strain gauge and SCALP are placed on opposite sides, additional reflections interfering with retardation measurement were observed. In order to minimize these interferences, the measuring depth of SCALP was reduced to 4 mm.

In these investigations SCALP-05 with an angle of $\alpha = 71.8°$ was used. The immersion Liqiud Code 5095 from Cargille Laboratories with a refractive index of 1.52 at a wavelength of 635 nm was used to minimize reflections at the surfaces between SCALP and the specimen. According to Anton (2015) the precision of SCALP is less than 5% for surface compression stresses greater than 20 MPa.

4.4 Data processing

For evaluation of the measured data, the retardation values were exported to MATLAB (2018). Only one of the three repetitions of each measured direction was

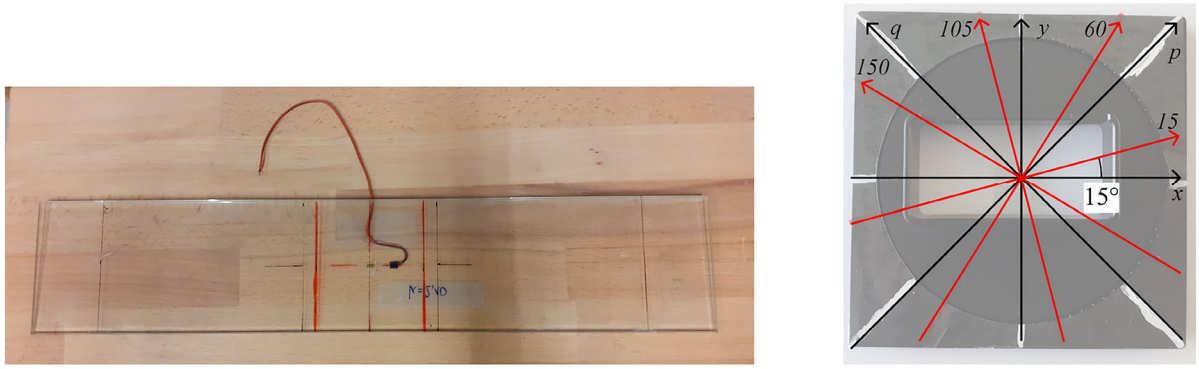

Fig. 3 **a** Specimen prepared with strain gauge and **b** coordinate system for setup 1 in black and for setup 2 (by 15° rotated coordinate system) in red, in the background the rotatable plate. ©Thiele

exported. Care was taken that the three repetitions show results with only small deviations.

With an own Script, a polynomic function of third order was identified by a least square fit so that the retardation values in depth 0.02–2.0 mm were described in the best way possible. As only surface stresses are investigated in this work, a polynomic function that is very close to the measured data in this range is of high interest. The retardation was fixed to zero at the glass surface. No other conditions were applied to the polynomic function.

Figure 4 shows three examples of measured retardations and fitted polynomic function for the three load cases of $\sigma_{add} = 0\,\text{MPa}$, $\sigma_{add} = 7.7\,\text{MPa}$ and $\sigma_{add} = 19.8\,\text{MPa}$ in four-point bending test described in Sect. 4.2. Measurement artifacts caused by the reflection of the laser on the surface can be seen in all three examples. During the experiment, the SCALP was placed on the specimen and only removed and replaced, when these artifacts became too large. In this way, deviations from measured positions were minimized, but with every rotation of the SCALP, a bit air entered the liquid between glass and SCALP and artifacts became larger. Additionally, the contact area between SCALP and glass specimen gets smaller with increasing applied load due to deflection.

The methods described in Sects. 3.1–3.3 process the derivatives of the identified third order polynomic functions. The photoelastic constant was determined to be 2.7 TPa^{-1} using the measured stresses in four-point bending test of specimen 5. This was also assumed for specimens 1 to 4.

5 Experimental results

In Sect. 5.1 results of measurements performed in four-point bending test evaluated with four of the five introduced methods are described. In Sect. 5.2 results of measurements performed on unloaded thermally tempered glass evaluated with the five methods introduced are described.

6 Fully tempered glass in four-point bending test

The measurements on thermally tempered glass with external load were evaluated using four of the described methods above. The first method described in Sect. 3.1 is not used, because due to the external load, which mainly acts in x-direction, no isotropic stress state is apparent. Here, $\sigma_y \neq \sigma_x \neq 0$ apply.

In Table 2, the principal stresses evaluated with the methods described in Sects. 3.2 and 3.3 as well as the standard deviation separately for σ_1 and σ_2 are given. The external load F measured with the load cell implemented in Zwick ROELL universal testing machine and resulting additional stress σ_{add} measured by the strain gauge are given for each load step. In Fig. 5, the evaluated principal stresses are shown for each load applied. Additionally, the addition of first principal stress and additional stress $(\sigma_1 - \sigma_{add})$ as well as a dashed line indicating first principal stress without external load are shown. Figure 5a shows the results for first setup (0°), Fig. 5b shows the results for second setup (15° rotated coordinate system).

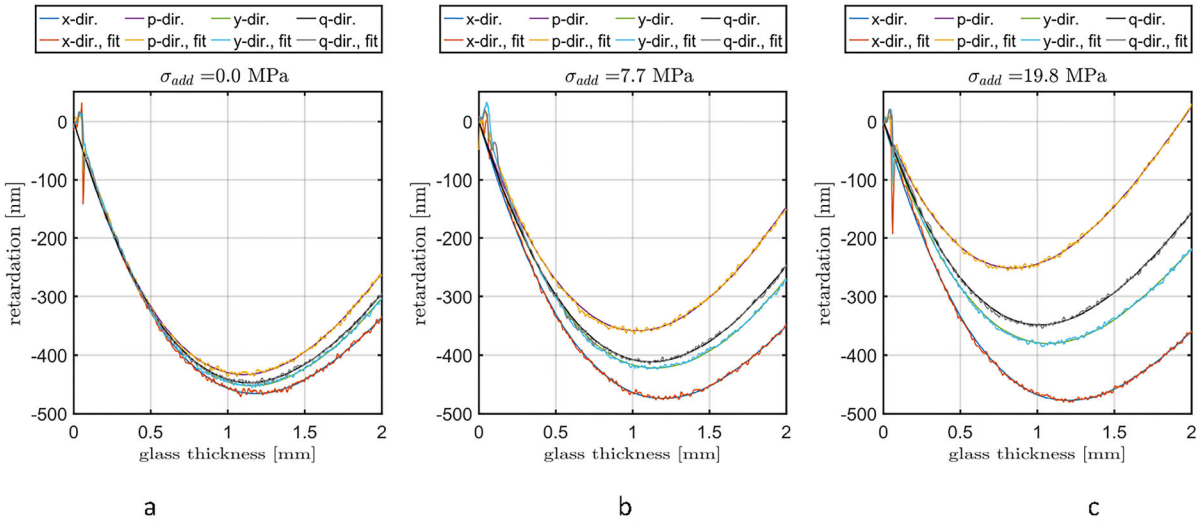

Fig. 4 Example of measured retardation and fitted polynomic functions in 4 point bending test: **a** $\sigma_{add} = 0$ MPa, **b** $\sigma_{add} = 7.7$ MPa, **c** $\sigma_{add} = 19.8$ MPa. ©Thiele

Table 2 Principal stresses for different external loads F leading to additional stress σ_{add} in x-direction evaluated by the four methods described in Sects. 3.2 and 3.3. For each load step principal stresses are given by using the coordinate system x–y as well as a 15° rotated coordinate system. Standard deviation separately for each principal stress is given

F	σ_{add}	Set-up	Section 3.2 Equation 9		Section 3.3a Equation 11–13		Section 3.3b Equation 14–16		Section 3.3c Equation 17–21		SD	
			σ_1	σ_2	σ_1	σ_2	σ_1	σ_2	σ_1	σ_2	σ_1	σ_2
[N]	[MPa]	[°]	[MPa]	[MPa]	[MPa]	[MPa]	[MPa]	[MPa]	[MPa]	[MPa]	[MPa]	[MPa]
0.0	0.0	0	−111.6	−113.0	−111.5	−113.0	−111.3	−113.3	−111.1	−113.5	0.2	0.2
		15	−112.7	−113.4	−112.3	−113.7	−111.9	−114.1	−111.7	−114.3	0.4	0.4
17.2	2.6	0	−106.0	−111.6	−106.0	−111.7	−105.8	−111.9	−105.1	−112.5	0.4	0.4
		15	−108.7	−111.7	−107.6	−112.8	−107.8	−112.6	−107.3	−113.1	0.6	0.6
26.4	3.9	0	−103.8	−111.7	−103.7	−111.8	−103.6	−111.9	−102.8	−112.7	0.5	0.5
		15	−104.8	−111.5	−104.0	−112.3	−104.2	−112.1	−103.4	−112.9	0.6	0.6
35.2	5.1	0	−103.4	−110.3	−103.4	−110.3	−102.6	−111.0	−101.7	−112.0	0.8	0.8
		15	−107.5	−110.8	−106.2	−112.0	−105.6	−112.6	−104.9	−113.4	1.1	1.1
55.1	7.9	0	−102.5	−114.3	−102.4	−114.4	−102.3	−114.5	−101.0	−115.8	0.7	0.7
		15	−103.1	−113.6	−102.8	−113.9	−102.9	−113.8	−101.7	−114.9	0.6	0.6
74.2	10.6	0	−98.4	−112.4	−98.4	−112.4	−98.3	−112.5	−96.8	−114.0	0.8	0.8
		15	−98.1	−107.9	−97.6	−108.4	−97.6	−108.4	−96.5	−109.5	0.7	0.7
111.4	15.8	0	−96.8	−111.9	−96.7	−112.0	−96.7	−112.0	−95.1	−113.6	0.8	0.8
		15	−97.0	−111.8	−96.0	−112.8	−95.7	−113.0	−93.9	−114.9	1.3	1.3
148.5	21.1	0	−91.0	−112.5	−91.0	−112.5	−90.9	−112.6	−88.6	−115.0	1.2	1.2
		15	−92.7	−111.0	−91.4	−112.3	−91.4	−112.2	−89.3	−114.4	1.4	1.4
186.5	26.4	0	−86.4	−112.8	−86.3	−112.9	−86.4	−112.8	−83.5	−115.8	1.5	1.5
		15	−87.3	−111.5	−85.8	−113.0	−85.3	−113.3	−82.6	−116.3	2.0	2.0

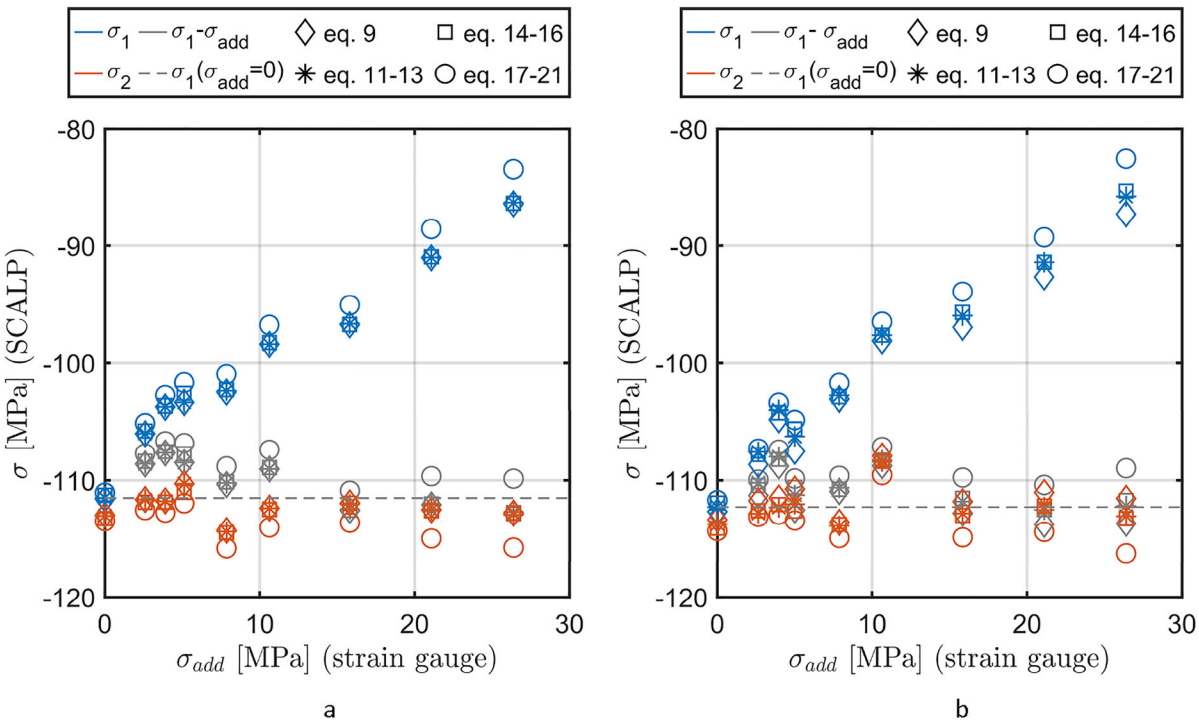

Fig. 5 Principal stresses evaluated for loaded thermally tempered glass: **a** evaluated stresses using measurements performed in setup 0° (x, p, y, q-directions) **b** evaluated stresses using measurements performed in setup 15° (15, 60, 105, 150-directions). ©Thiele

From Table 2, it can be seen that standard deviation increases up to 2.0 MPa with increasing external load and thus increasing difference of σ_1 and σ_2. When looking at Fig. 5a, only the principal stresses evaluated with the simplified method (Eqs. 17–21) overestimates the first principal stress and underestimates the second principal stress. This deviation is larger for larger applied loads. The three remaining methods show results in good agreement. When looking at Fig. 5b the results of the four methods deviate more. The simplified method (Eqs. 17–21) still overestimates the first principal stress und underestimates the second principal stress. The method given in Eq. 9, which assumes that measured directions equal to principal stress directions, underestimates first principal stress and overestimates second principal stress. The method using three measured directions (Eqs. 14–16) and the method using four measured directions (Eqs. 11–13) show similar results.

In both setups the addition of first principal stress and additional stress ($\sigma_1 - \sigma_{add}$) are close to first principal stress without external load for large applied stresses ($>$ 15 MPa). For small applied stresses ($<$ 15 MPa), the results differ to first principal stress. If the direction of the first principal stress of the stress state in the thermally tempered glass is the same as the direction of the first principal stress in the four-point bending test, the addition would be expected to be equal to the first principal stress without load. If this is not the case, a difference between the addition and the first principal stress is to be expected and, at least for small loads, the principal stress directions cannot be assumed to be known before measurement.

In Fig. 6 the azimuth relative to the x-axis, which was parallel to the longer side of the specimen, of the first principal stresses are shown. In Fig. 6a the results of setup 1 (0°) are shown, in Fig. 6b the results of setup 2 (15°) are shown. Since for setup 2, the angles are calculated relative to the measuring direction 15 (see Fig. 3b), this difference was subtracted so that the data in Fig. 6b show the angle relative to the x-axis. An additional line shows the shifted reference line for setup 2.

When looking at Fig. 6, the angles evaluated with the different methods described in Sect. 3 show similar results for setup 2. For setup 1, the method using

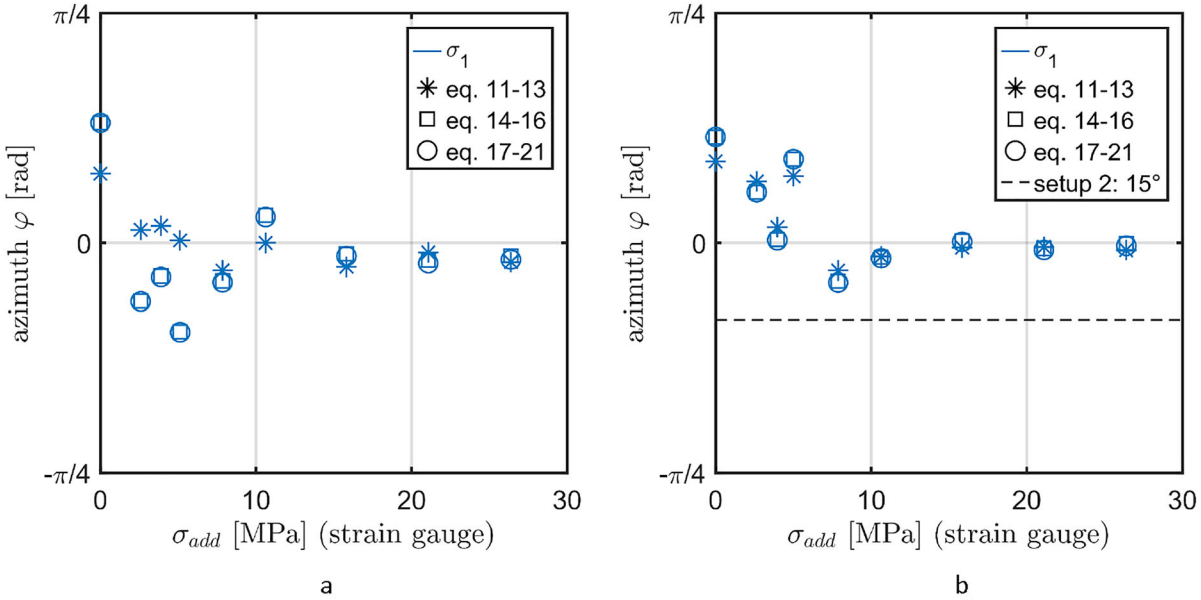

Fig. 6 Azimuth of principal stress directions relative to the x-axis (long side of specimen) evaluated for loaded thermally tempered glass: **a** evaluated stress directions using measurements performed in setup 0° (x, p, y, q-directions) **b** evaluated stress directions using measurements performed in setup 15° (15, 60, 105, 150-directions). ©Thiele

four measured directions (Eqs. 11–13) show deviating results for measurements with small external loads compared to the method using three measured directions (Eqs. 14–16) and the simplified method (Eqs. 17–21). The measurement without external load shows a principal stress direction relative to the x-axis of $0.13\pi = 23.4°$ (Eq. 14–21), respectively $0.07\pi = 12.6°$ (Eqs. 11–13), in setup 1 and $0.11\pi = 19.8°$ (Eqs. 14–21), respectively $0.09\pi = 16.2°$ (Eqs. 11–13), in setup 2. For small external stresses ($0\ \text{MPa} < \sigma_{add} < 15\ \text{MPa}$), the angles evaluated are closer to the x-axis. As expected, the direction of first principal stress equals to the x-axis for large applied loads. Measurements in both setups support this expectation.

In Fig. 7, the differences of principal stresses measured with SCALP-05 and stress measured with strain gauge are compared. As the stress state of thermally tempered glass must not be isotropic, the difference of principal stress with $F = 0$ is subtracted, see Eq. 22.

$$\Delta\sigma_i(F) = \sigma_{1,i}(F) - \sigma_{2,i}(F) - \left(\sigma_{1,i}(F=0) - \sigma_{2,i}(F=0)\right) \quad (22)$$

Herein, the index i indicates the chosen evaluation method. This is a simplification, as first principal stress direction of the residual stresses within thermally tempered glass and first principal stress direction of additional stresses due to the applied load must not be equal (see Fig. 6). Transverse strain was not measured and additional stresses in transverse direction due to external load are neglected.

In Fig. 7a, the results evaluated by Eqs. 9 and 17–21, in Fig. 7b the results evaluated by Eqs. 11–13 and Eqs. 14–16 are shown. Ideally, the measured stress difference $\Delta\sigma$ equal the measured external stress σ_{add}. The function $y = x$ is added to the plot to visualize the ideal result. The photoelastic constant was chosen to $C = 2.7\,\text{TPa}^{-1}$ in order to minimize this difference.

Compared to the results displayed in Fig. 7b, the results displayed in Fig. 7a show larger deviations from the ideal curve. Also, deviations of the results evaluated in setup 2 compared to the results evaluated in setup 1 can be observed. These deviations are larger for the results shown in Fig. 7a.

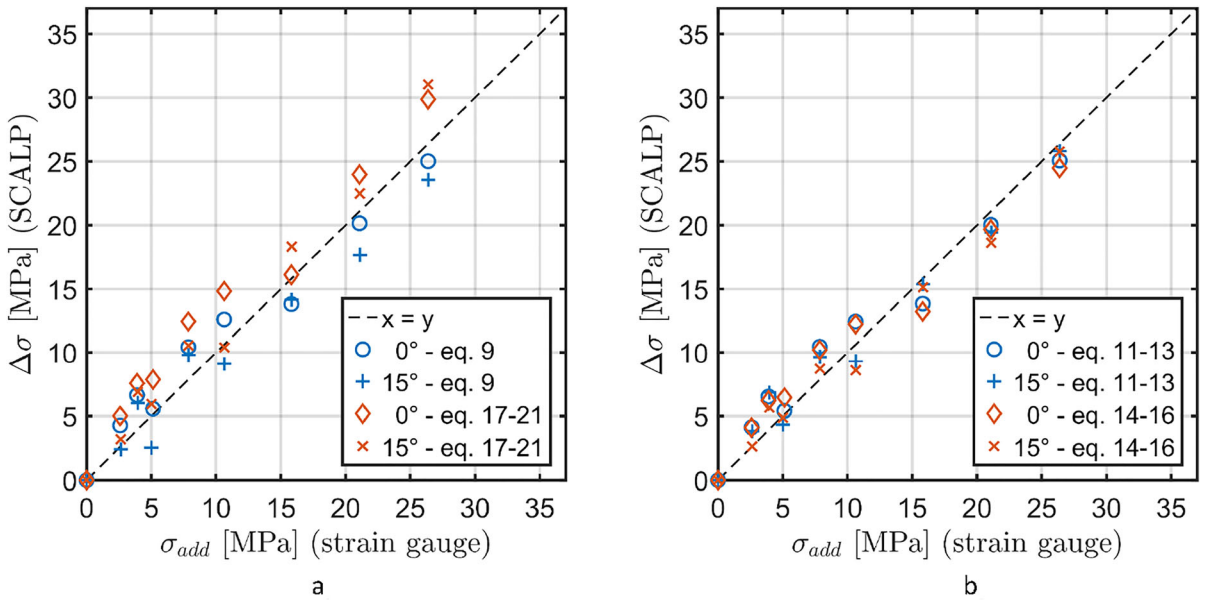

Fig. 7 Principal stress differences $\Delta\sigma$ evaluated by Eq. (22) and additional stress measured with strain gauge. Photoelastic constant is chosen to $C = 2.7\text{TPa}^{-1}$. ©Thiele

6.1 Fully tempered glass without external load

The four specimens investigated without external load, were measured at 21 positions per specimen. For the comparison of the different methods, only 6 positions per specimen are used. Therefore, three points close to isotropic stress state ($\sigma_1 - \sigma_2 < 3\,\text{MPa}$) and three points with larger differences ($3\,\text{MPa} < \sigma_1 - \sigma_2 < 6\,\text{MPa}$) were chosen per specimen. In Table 3, the principal stresses evaluated with the methods described in Sects. 3.1 to 3.3 as well as the standard deviation separately for σ_1 and σ_2 are given. For the method assuming isotropic stress state (Eq. 7), four values could be evaluated. Here, only minimum and maximum of these four values are given. As this method assumes isotropic stress state ($\sigma_1 = \sigma_2$), both values are included in the standard deviation for σ_1 and σ_2. For the method assuming known principal stress directions (Eq. 9), x-and y-directions were chosen to be evaluated. In Fig. 8, the evaluated principal stresses are shown. Figure 9 shows the evaluated azimuth relative to the x-axis corresponding to the first principal stress for each measurement.

From Table 3 and Fig. 8, it can be seen that standard deviations for the points close to isotropic stress state are smaller ($0.5\,\text{MPa} - 1.2\,\text{MPa}$) than standard deviations for the points with larger stress differences ($1.4\,\text{MPa} - 2.8\,\text{MPa}$). When looking at Figs. 8 and 9, it becomes clear that the stress states evaluated are not isotropic and most of the measured points show principal stress directions that do not equal the assumed principal stress directions (x- and y-direction, 0° and 90°).

The highest deviations are observed for stresses evaluated with the method assuming isotropic stress state (Eq. 7). Minimum and Maximum of the four evaluated stresses using this method fit mostly well to the two principal stresses evaluated with the other methods. If only one measurement of this method is available, the evaluated stress can only be interpreted as a rough reference value.

The second highest deviations are observed for the method assuming known principal stress directions (Eq. 9). Most of the selected measured points in this work show principal stress directions deviating from measured directions. Comparing Figs. 8 and 9, the deviations of the results are independent of the evaluated principal stress direction but depend on the found principal stress differences. Figure 8 shows that results evaluated with this method are in good agreement with results evaluated with other methods for lower stress differences. The results for measured points with larger stress differences deviate with results of other methods.

The third highest deviations regarding principal stresses are observed for stresses evaluated with the

Table 3 Evaluated principal stresses for measurements on thermally tempered glass without external load. Standard deviation separately for each principal stress is given. For each of the four specimens, the first three rows show low difference of principal stress, the second three rows show larger differences

No.	Section 3.1 Equation (7)		Section 3.2 Equation (9)		Section 3.3a Equation (11–13)		Section 3.3b Equation (14–16)		Section 3.3c Equation (17–21)		SD	
	Min [MPa]	Max [MPa]	σ_1 [MPa]	σ_2 [MPa]	σ_1 [MPa]	σ_2 [MPa]	σ_1 [MPa]	σ_2 [MPa]	σ_1 [MPa]	σ_2 [MPa]	σ_1 [MPa]	σ_2 [MPa]
1	−106.2	−103.2	−103.4	−105.9	−103.4	−105.9	−103.4	−105.9	−103.1	−106.2	1.2	1.2
2	−106.1	−103.8	−104.0	−105.9	−104.0	−105.9	−104.0	−105.9	−103.8	−106.1	0.9	0.9
3	−104.2	−102.9	−103.7	−104.1	−103.6	−104.2	−103.1	−104.7	−102.9	−104.9	0.5	0.7
4	−107.3	−102.8	−103.1	−106.2	−102.6	−106.8	−102.1	−107.3	−101.5	−107.9	2.1	1.8
5	−106.8	−103.3	−104.0	−106.5	−103.3	−107.1	−103.5	−107.0	−103.1	−107.4	1.4	1.5
6	−106.2	−100.6	−102.7	−103.6	−100.8	−105.5	−100.6	−105.7	−100.0	−106.3	2.3	2.2
7	−110.7	−108.0	−108.2	−110.4	−108.1	−110.5	−108.2	−110.5	−107.9	−110.7	1.1	1.1
8	−112.1	−109.6	−109.8	−111.9	−109.6	−112.1	−109.7	−112.0	−109.4	−112.2	1.0	1.0
9	−108.4	−105.5	−107.2	−108.2	−106.6	−108.8	−107.2	−108.3	−107.1	−108.4	0.9	1.2
10	−113.9	−110.0	−110.9	−112.5	−109.9	−113.5	−110.1	−113.3	−109.7	−113.6	1.6	1.4
11	−113.8	−108.9	−109.6	−111.8	−108.5	−113.0	−108.9	−112.5	−108.5	−112.9	2.0	1.7
12	−109.2	−102.8	−103.4	−108.6	−103.3	−108.7	−103.3	−108.7	−102.8	−109.3	2.5	2.5
13	−54.9	−52.6	−52.7	−54.4	−52.5	−54.6	−52.2	−54.9	−51.9	−55.2	1.1	1.0
14	−53.7	−51.0	−51.2	−53.5	−51.2	−53.6	−51.1	−53.6	−50.9	−53.9	1.1	1.1
15	−52.9	−50.0	−50.3	−52.6	−50.3	−52.6	−50.1	−52.8	−49.8	−53.0	1.2	1.1
16	−53.0	−47.9	−50.3	−52.4	−49.0	−53.7	−49.6	−53.1	−49.2	−53.5	1.7	2.2
17	−55.4	−49.1	−49.6	−54.8	−49.6	−54.9	−49.4	−55.0	−48.9	−55.6	2.5	2.5
18	−56.2	−49.4	−53.0	−54.3	−50.8	−56.6	−51.4	−55.9	−51.0	−56.4	2.4	2.8
19	−38.2	−36.1	−36.2	−37.2	−35.7	−37.7	−35.3	−38.1	−35.1	−38.4	1.1	0.9
20	−35.3	−31.9	−32.6	−35.1	−32.4	−35.3	−32.6	−35.1	−32.3	−35.3	1.2	1.4
21	−35.0	−33.1	−33.3	−34.9	−33.3	−34.9	−33.2	−34.9	−33.0	−35.1	0.8	0.8
22	−41.1	−37.4	−37.7	−40.7	−37.7	−40.8	−37.7	−40.8	−37.4	−41.1	1.4	1.4
23	−41.3	−37.1	−37.5	−40.9	−37.3	−41.2	−37.1	−41.3	−36.7	−41.8	1.7	1.7
24	−43.7	−38.5	−39.0	−43.2	−38.5	−43.7	−38.7	−43.5	−38.2	−44.0	2.1	2.1

simplified method (Eqs. 17–21), see Fig. 8. Regarding the principal stress directions, this method is in good agreement with the method using three measured directions (Eqs. 14–16), but deviate from the method using four measured directions, see Fig. 9.

7 Conclusion

In Sect. 3 different methods for evaluating principal stresses with measured data using SCALP are introduced. Firstly, a method assuming isotropic stress state which only need one measured direction to identify principal stresses is described. Secondly, a method using measurements in principal stress directions is introduced. In Sect. 3.3 two methods using three measured directions and a method using 4 measured directions are described. In order to compare these methods, principal stresses were evaluated by four methods for 18 stress states in four-point bending test and by five methods for unloaded thermally tempered glass.

Summarizing the measurements in four-point bending test, these measurements show that the results evaluated with the method assuming known principal stress

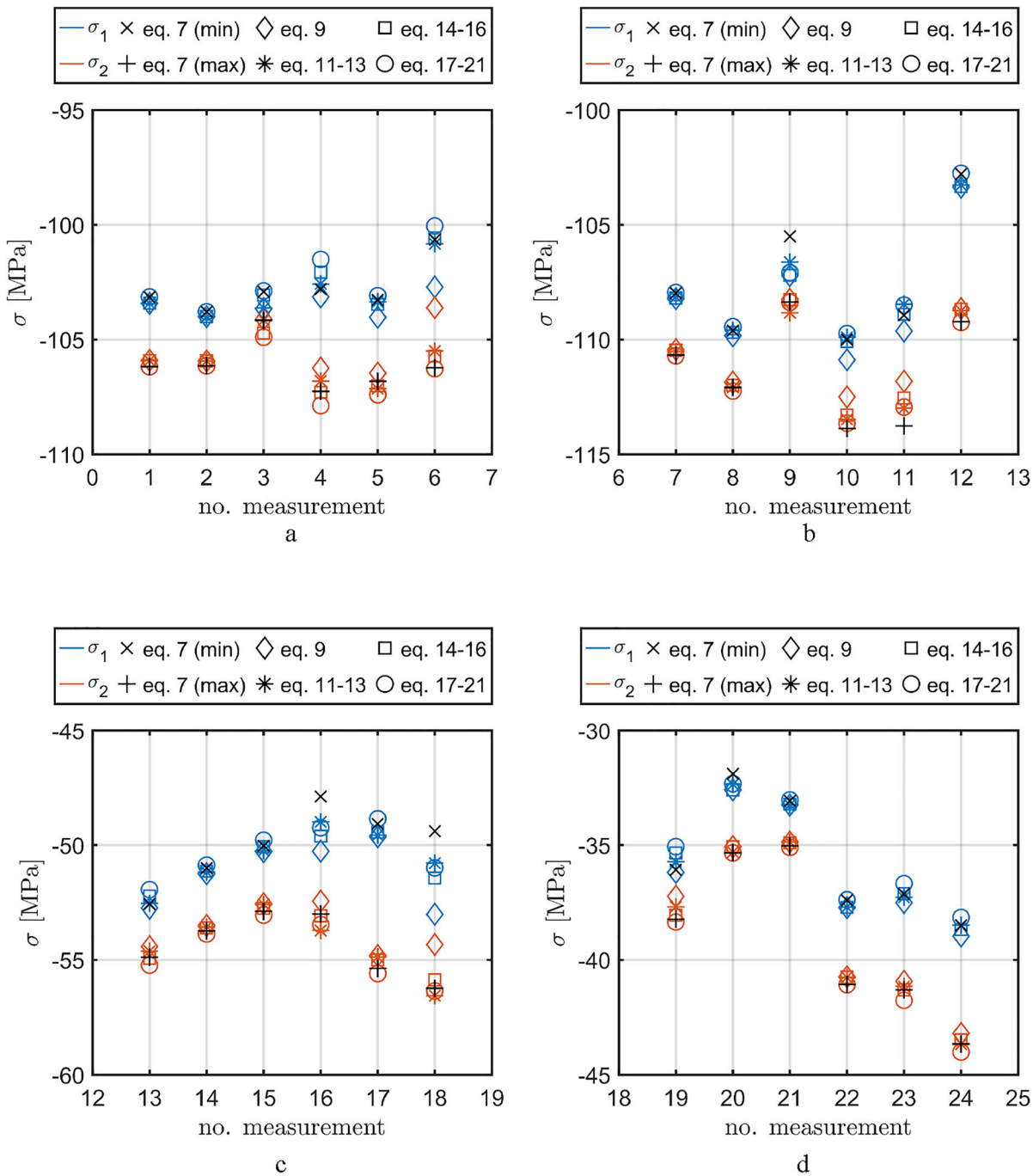

Fig.8 Principal stresses evaluated for unloaded thermally tempered glass: **a** specimen 1, **b** specimen 2, **c** specimen 3, **d** specimen 4. X-axis refers to number of measurements in Table 3.©Thiele

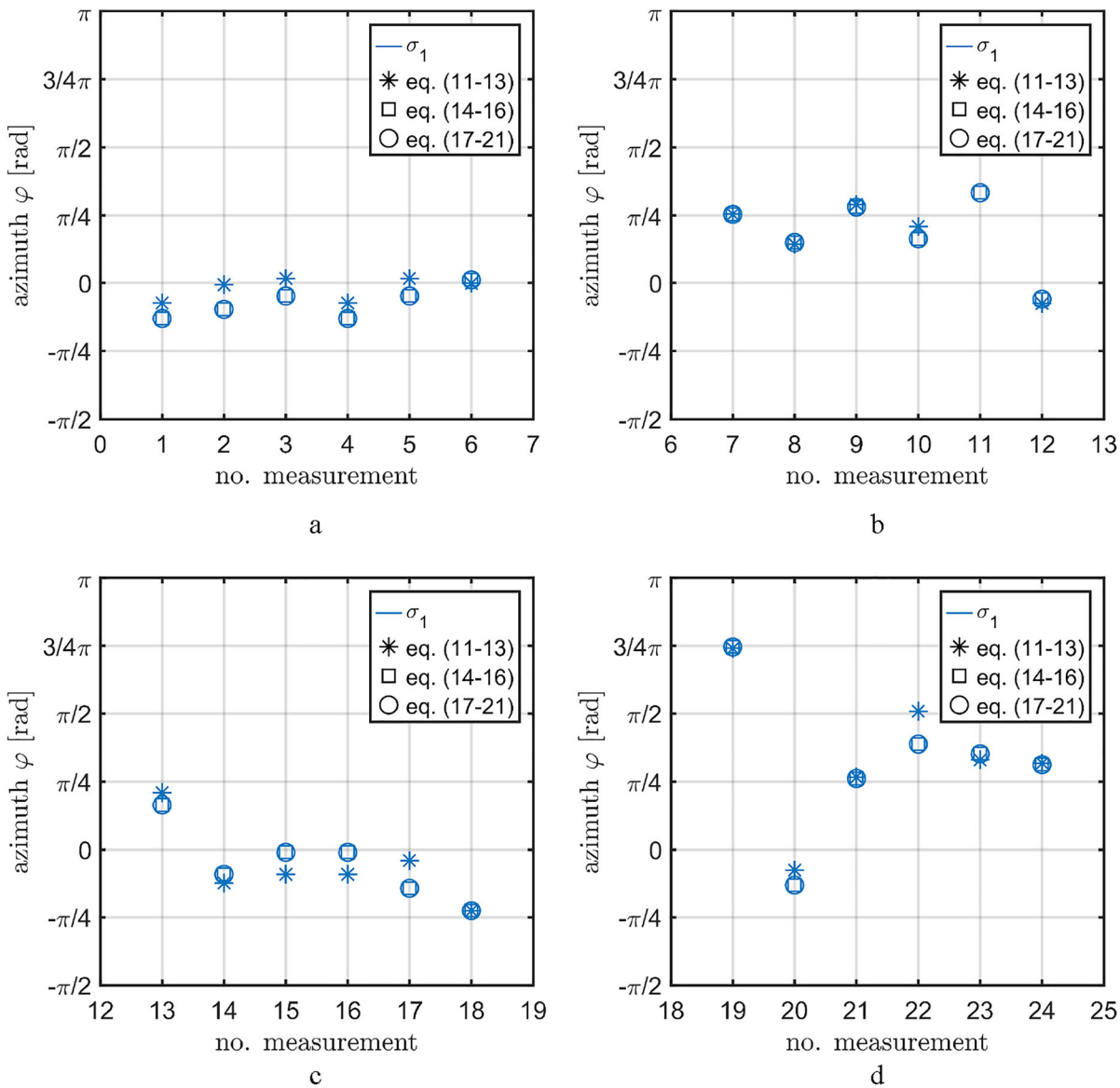

Fig.9 Azimuth relative to x-axis corresponding to first principal stress evaluated for unloaded thermally tempered glass: **a** specimen 1, **b** specimen 2, **c** specimen 3, **d** specimen 4. X-axis refers to number of measurement in Table 3.©Thiele

directions (Eq. 9) show results in good agreement with the other methods, when the principal stress directions are assumed correctly (setup 1). For the case of incorrectly assumed principal stress direction, as simulated with setup 2, the results deviate from results evaluated with other methods. This fits well with the theory described in Sect. 3.1. As for this method the measured directions are assumed to be equal to the principal stress directions, the contribution of τ_{xy} is neglected, see Eq. 5. In setup 1 this is the case, in setup 2 this is not the case.

The method using four measured directions (Eqs. 11–13) and the method using three measured directions (Eqs. 14–16) show similar results, independently of the setup, regarding principal stresses. Regarding evaluated principal stress directions, the results deviate independently of the setup. Both methods are able to identify the non-isotopic stress state with unknown principal stress directions. Little deviations

regarding principal stresses are to be expected. For the method using four measured directions, the contribution of τ_{xy} is neglected, when evaluating the stresses $\sigma_x, \sigma_p, \sigma_y$ and σ_q. The method using three measured directions (Eqs. 14–16) does not neglect τ_{xy} when evaluating the principal stresses. It is not clear which of the methods give results with higher accuracy.

For the simplified method the deviations of principal stresses are larger with larger applied load independently of the setup. The evaluated principal stress directions are in good agreement with method using three measured directions (Eqs. 14–16). The higher deviations in principal stresses result, because when evaluating σ_x, σ_p and σ_y, isotropic stress states are assumed for each measurement. The agreement in principal stress directions with the method using three measured directions (Eqs. 14–16) could follow from the fact that the same 3 measurements are used here.

Overall, the methods that include more assumptions that reduce complexity of the task, show larger deviations to the methods that include less assumptions. Standard deviations for the measurements in four-point bending test do not exceed 2.0 MPa.

Also, for measurements on unloaded thermally tempered glass, methods including more assumptions to reduce complexity of the task, show larger deviations. The highest deviations shows the method assuming isotropic stress state (Eq. 7), followed from the method assuming known principal stress directions (Eqs. 11–13). The simplified method (Eq. 17–21) shows deviations, which are smaller to the methods named above. Standard deviations regarding the different evaluation methods do not exceed 2.8 MPa.

As a conclusion, the user should think about the current stress state and principal stress directions before performing SCALP measurements. In dependency of needed accuracy of the measurement and available time, an evaluation method can be chosen. The more directions need to be measured, the more time is necessary. By assuming an isotropic stress state, only one direction must be measured, but the result could over- or underestimate the current stress state.

In this work evaluated stresses using the methods described in Sects. 3.3a and b showed good agreement. Advantage of the method described in Sect. 3.3b is, that only three measured directions are needed in comparison to four measured directions. The simplified method described in Sect. 3.3c showed larger deviations from expected results. This shows, that the retardation measured always depends on principal stresses in the plane perpendicular to the laser beam and not just on the stress perpendicular to measured direction. Care should be taken when SCALP measurements are interpreted.

In the experience of the authors, deviations because of badly fitted polynomic functions and the conditions applied to this function have a large influence on evaluated stress. Also, large reflections on glass surface can lead to higher deviations. In order to get good measurement results, care should always be taken to reduce theses errors.

Acknowledgements The results were developed within the WIPANO project "Bewertungskriterien zur Normung von Anisotropie-Effekten bei thermisch vorgespanntem Flachglas" funded by the german federal ministry for economic affairs and energy (BMWi).

Funding Open Access funding enabled and organized by Projekt DEAL.

References

Aben, H., Guillemet, C.: Photoelasticity of Glass. Springer, Berlin (1993)

Aben, H., Anton, J., Errapart, A.: Modern photoelasticity for residual stress measurement in glass. Strain **44**, 40–48 (2008)

Anton, J., Aben, H.: A compact scattered light polariscope for residual stress measurement in glass plates. In: Glass Processing Days, pp. 86–88. Tampere, UK (2003)

Anton, J.: Scattered Light Polariscope SCALP Instruction manual Ver. 5.8.2. (2015) Talinn, Estonia: GlasStress Ltd.

Chen, Y., Lochegnies, D., Defontaine, R., Anton, J., Aben, H., Langlais, R.: Measuring the 2D residual surface stress mapping in tempered glass under the cooling jets: the influence of process parameters on the stress homogeneity and isotropy. Strain **49**(1), 60–67 (2013). https://doi.org/10.1111/str.12013

DIN SPEC 18198:2022-05: Messung und Bewertung von optischen Anisotropie-Effekten bei thermisch vorgespanntem Glas. Beuth, Berlin (2022)

Dix, S., Efferz, L., Sperger, L., Schuler, C., Feirabend, S.: Analysis of residual stresses at holes near edges in tempered glass. Ce papers **4**, 145–162 (2021a). https://doi.org/10.1002/cepa.1628

Dix, S., Müller, P., Schuler, C., Kolling, S., Schneider, J.: Digital image processing methods fort he evaluation of optical anisotropy effects in tempered architectural glass using photoelastic measurements. Glass Struct. Eng. **6**, 3–19 (2021b). https://doi.org/10.1007/s40940-020-00145-3

Dix, S., Schuler, C., Kolling, S.: Digital full field photoelasticity of tempered architectural glass: a review. Opt. Lasers Eng. (2022). https://doi.org/10.1016/j.optlaseng.2022.106998

Errapart, A., Anton, J.: Photoelastic residual stress measurement in nonaxisymmetric glass containers. In EPJ Web Conf. **6**, 32008 (2010). https://doi.org/10.1051/epjconf/20100632008

Fachverband Konstruktiver Glasbau e.V.: The visual quality of glass in building – anisotropies in heat treated flat glass. Technical Note FKG 01/2019. (2019)

Gross, D., Hauger, W.,Schröder, J., Wall, W.A.: Technische Mechanik 2. (2014)

Karvinen, R., Aronen, A.: Influence of Cooling Jets on Stress Pattern and Anisotropy in Tempered Glass. Glass Performance Days (2019), pp. 212-215

Lohr, K.: Thermisch vorgespanntes Glas mit nachgeschliffenen Kanten. (2020) https://nbn-resolving.org/urn:nbn:de:bsz:14-qucosa2-706717

MATLAB: version R2018a. (2018). Massachusetts: The MathWorks Inc

Nielsen, J.H., Olesen, J.F., Stang, H.: Characterization of the residual stress state in commercially fully tempered glass. J. Mater. Civ. Eng. (2010). https://doi.org/10.1061/(ASCE)0899-1561(2010)22:2(179)

Nielsen, J.H., Thiele, K., Schneider, J., Meyland, M.J.: Compressive zone depth of thermally tempered glass. Constr. Build. Mater. (2021). https://doi.org/10.1016/j.conbuildmat.2021.125238

Pour-Moghaddam, N.: On the fracture Behaviour and the fracture Pattern Morphology of Tempered Soda-Lime Glass. Springer, Cham (2019). https://doi.org/10.1007/978-3-658-28206-6

Schneider, J., Kuntsche, J., Schula, S., Schneider, F., Wörner, J.D.: Glasbau Grundlagen Berechnung. Konstruktion. (2016). https://doi.org/10.1007/978-3-540-68927-0

Thiele, K., Kraus, M., Schneider, J., Nielsen, J.H.: Statistische Charakterisierung der Verteilung der Druckzonentiefe vorgespannter Gläser. Glasbau 2022

Zaccaria, M., Overend, M.: Nondestructive safety evaluation of thermally tempered glass. J. Mater. Civil Eng. **32**(4), 04020043 (2020). https://doi.org/10.1061/(ASCE)MT.1943-5533.0003086

Zeidler, E.: Springer-Taschenbuch Der Mathematik. (2013). https://doi.org/10.1007/978-3-8348-2359-5